Cross-plane thermal conductivity of self-assembled Ge quantum dot superlattices

J. L. Liu*

Department of Electrical Engineering, University of California at Riverside, Riverside, California 92521

A. Khitun and K. L. Wang

Device Research Laboratory, Department of Electrical Engineering, University of California at Los Angeles,
Los Angeles, California 90095-1594

W. L. Liu

Nanoscale Heat Transfer and Thermoelectrics Laboratory, Mechanical and Aerospace Engineering Department,
University of California at Los Angeles, Los Angeles, California 90095-1594

G. Chen

Mechanical Engineering Department, Massachusetts Institute of Technology, Cambridge, Massachusetts 02139

Q. H. Xie

Process and Materials Characterization Laboratory, Digital DNA Laboratories, Motorola, 2100 E. Elliot Rd., Tempe, Arizona 85284

S. G. Thomas

Si RF/IF Technologies, Digital DNA Laboratories, Motorola, 2100 E. Elliot Rd., Tempe, Arizona 85284
(Received 9 December 2002; published 30 April 2003)

We report the temperature dependent cross-plane thermal conductivities of Ge quantum dot superlattices measured by the 3ω method. A large reduction in the thermal conductivity of the superlattices compared with that of bulk materials is observed. A simple model taking into account the relaxation time approximation, including phonon scattering on quantum dots, well explains the experimental data.

I. INTRODUCTION

The self-assembled quantum dot structure is an interesting topic for physical investigation of zero-dimensional system. Due to the low-dimensional confinement effect, the Ge-on-Si quantum dot structure is expected to demonstrate novel optoelectronic properties that can be applied to develop Si-based technology competitive with traditional optoelectronic materials such as III-V compounds.[1–5] In addition, it is predicted that low-dimensional systems can have a thermoelectric figure of merit, Z, much larger than that of bulk material due to enhanced electron transport and reduced thermal conductivity.[6] Studies of Z enhancement stimulated by this prediction have been carried out on several material systems.[7–13] Progress to date in Si/Ge quantum well superlattice material system indicated that Z enhancement in both in-plane and cross-plane directions can be realized.[7,11,13] Furthermore, due to its δ-like density of states, quantum dot structures are believed to have better Z enhancement than quantum wells. This was initially verified using the PbTe superlattice system.[10] For the SiGe quantum dot system, there have been several studies on the phonon spectrum on Ge dot superlattices,[14,15] though limited work has been done on the thermal transport properties of the Ge quantum dots.[16,17] In this paper, we report systematically the investigation of cross-plane thermal conductivity of Ge quantum dot superlattices.

II. EXPERIMENT

Samples (*A* through *G*) were grown by a solid source molecular beam epitaxy (MBE) system on Si(100) sub-strates. The nominal growth rates were 1 and 0.2 Å/s for Si and Ge, respectively. The growth started with a 100-nm Si buffer layer, followed by the quantum dot superlattice layers that are composed of bilayers in which the Ge dot layers are separated by a 20-nm Si spacer layer. The periods and nominal Ge thickness are different for various samples. Most of the samples investigated here are also described in Ref. 18, where we systematically studied phonons in the Ge quantum dot superlattices. To investigate structural properties of the samples, transmission electron microscopy (TEM) and atomic force microscopy (AFM) were used. Figure 1(a) shows a typical cross-sectional TEM image of sample C. The 10-period vertically correlated Ge quantum dot layers are evident. Figure 1(b) shows an AFM image of sample C. All dots appear as domes and pyramids. The density is 4.1 $\times 10^9$ cm^{-2}. The average dot base and height were determined to be 14 and 122 nm, respectively. Here, the AFM tip effect on the dot size quantification has been calibrated by TEM and taken into account. Similar measurements have been performed on other samples as well. The structural data are summarized in Table I.

Thermal conductivity of the samples was measured by a differential 3ω method.[19,20] The reference sample used for differential measurement is the same as the substrate used in sample growth. On each sample, a plasma-enhanced chemical vapor deposited (PECVD) silicon nitride layer, about 100 nm thick, was deposited to provide electrical insulation for the measurement. Gold 3ω heater-thermometer wires were patterned and fabricated on top of the nitride layer. The mea-

FIG. 2. Thermal conductivity as a function of temperature for quantum dot sample C and bulk single-crystal Si and Ge.

tivities of the nitride layer and the Si substrate as a way of checking the accuracy of measurement.

III. RESULTS AND DISCUSSIONS

Figure 2 shows the thermal conductivity versus measurement temperature for sample C and bulk Si and bulk Ge. A large reduction in the cross-plane thermal conductivity of the quantum dot sample as compared with the value of the bulk Si and Ge samples is observed. The peak value on the K-T curve shifts to a temperature as high as about 200 K, compared with about 10–30 K for bulk material. This is a typical indication of the quantum size effect. Figure 3 shows the thermal conductivity as a function of measurement temperature for all the samples. For the group of samples grown at 540 °C, the data above 200 K shows that with the increase in Ge dot size, the thermal conductivity decreases. This trend is not obvious for the data below 200 K, mainly because of the relatively small thickness of the samples grown at 540 °C (10 periods). A similar trend is also observed for the group of samples grown at 600 °C. For the samples with the same Ge equivalent thickness but grown at different temperatures (A, C, and E), the results show that the higher the growth temperature, the larger the thermal conductivity. Figure 4 sum-

FIG. 1. (a) TEM image of sample C; (b) AFM image of sample C.

surements were conducted inside a vacuum cryostat that operated from 80 to 300 K. For each temperature point, a wide frequency range, from 300 to 5000 Hz, is adopted in the temperature rise signal sampling. The thermal conductivity in the cross-plane direction is obtained from a fitting program, which can also be used to extract the thermal conduc-

TABLE I. Structural data of the samples.

Sample	Growth T (°C)	Period	Ge layer Thickness (Å)	Si layer Thickness (nm)	Dot base (nm)	Dot height (nm)	Density (cm^{-2})
A	500	10	15	20	114.7	15.1	5.9×10^8
B	540	10	12	20	110.4	11.9	3.6×10^9
C	540	10	15	20	122.0	14.0	4.1×10^9
D	540	10	18	20	122.2	16.0	3.5×10^9
E	600	22	15	20	175.5	10.2	2.6×10^8
F	600	22	12	20	152.4	10.0	1.4×10^8
G	600	25	6	20	—	—	—
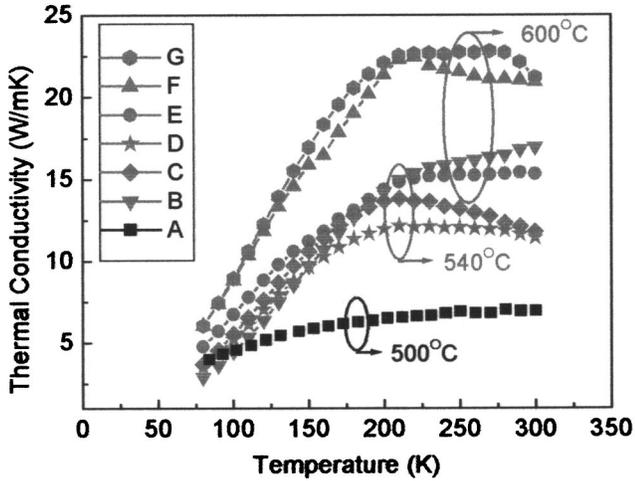
FIG. 3. Thermal conductivity as a function of temperature for samples grown at different temperatures and with different Ge equivalent thicknesses.

marizes the room-temperature thermal conductivity as a function of the nominal Ge layer thickness. Error bars represent the fluctuations among the values from measurements at different times and for wires having different sizes. Line 1 shows that there is a slight dependence of thermal conductivity on nominal Ge thickness for the samples grown at the same substrate temperature. Line 2, however, suggests that for the same nominal Ge layer thickness, there is a much more significant change in thermal conductivity for the samples grown at the different substrate temperatures.

In order to explain the above results, we realize that the expression for the lattice thermal conductivity in the relaxation-time approximation can be written as[21,22]

$$\kappa = \frac{1}{3} \sum_i \int dk \, v_{g_i}^2(k) \tau_{C_i}(k) S_i(k),\tag{1}$$

where i denotes a particular phonon polarization branch, $v_{g'_i}$ is the phonon group velocity associated with the ith branch, τ_C is the combined relaxation time, and $S_i(k)dk$ is the contribution to the specific heat from modes of the polarization
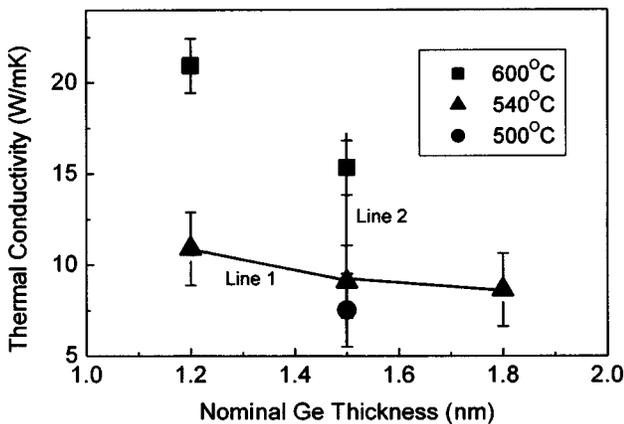
FIG. 4. Room-temperature thermal conductivity as a function of nominal Ge thickness.

branch i in the phonon wave vector interval of $k \, dk$. The combined relaxation time τ_C includes all relaxation rates corresponding to the different scattering processes, which do not conserve crystal momentum:[22]

$$\frac{1}{\tau_C} = \sum \frac{1}{\tau} = \frac{1}{\tau_M} + \frac{1}{\tau_B} + \frac{1}{\tau_U} + \frac{1}{\tau_D}.\tag{2}$$

Here, $1/\tau_U$ is the three-phonon umklapp processes, $1/\tau_M$ is the phonon–point-defect scattering (isotopes, impurities, etc.), $1/\tau_B$ is the phonon-boundary scattering, and $1/\tau_D$ is the phonon scattering by quantum dots.[23] Equation (2) includes the phonon relaxation processes, which are dominant in Si, Ge, and Si_xGe_{1-x} structures. The expressions for phonon relaxation rates $1/\tau_U$, $1/\tau_M$, and $1/\tau_B$ were derived by Klemens in Ref. 22. The new term $1/\tau_D$ is related to the phonon scattering on quantum dots. The most general expression for the phonon scattering rate on quantum dots can be written as

$$\frac{1}{\tau_D} = \frac{v_g \sigma_V}{V},\tag{3}$$

where σ_V is the total cross section of the dot ensemble of volume V. Here, we treat all dots as equal spheres with radius a on a plane, which is perpendicular to the growth direction. To describe the phonon transport in quantum dot superlattices, we use the continuum model approximation and an assumption that the thermal phonon wave can be represented by a sum of plane waves.[23] Thus, the expression for the scattering cross section σ of a single quantum dot becomes[24]

$$\sigma = \frac{\pi}{k^2} \sum_{m=0}^{\infty} (2m+1)|1+R_m|^2.\tag{4}$$

In the above equation, R_m is a reflection coefficient

$$R_m = \frac{h'^*_m(ka) + i\beta h^*_m(ka)}{h'_m(ka) + i\beta h_m(ka)},\tag{5}$$

where

$$\beta = i \frac{\rho c}{\rho_e c_e} \left[\frac{j'_m(ka)}{j_m(k_e a)} \right],$$

ρ is the density, c is the sound velocity, the subscript e denotes the parameter of the dot material, $h_m(ka) = j_m(ka) + iy_m(ka)$, j and y are the spherical Bessel functions of the first and second kinds, respectively, and h^*_m is the complex conjugate. Because of Si/Ge interdiffusion, the quantum dots are not pure Ge. Average Ge compositions were obtained by Raman scattering for these quantum dot samples.[18] The particular density and sound velocity inside a dot are modified by the Ge composition in the quantum dot. We use an approximate formula $\rho_e = \rho_{Ge} x + (1-x)\rho_{Si}$ and $c_e = c_{Ge} x + (1-x)c_{Si}$, where x is the Ge composition.

In order to find final σ_V, we have to sum the contributions from all scattered waves from all the dots in the unit volume V, taking into account dot ordering in the layers. At

some arbitrary point, the reflected amplitude S normalized to the amplitude of the incident plane wave is given as

$$S = \frac{|F(\vartheta)|^2}{r^2} \sum_{n=1}^{N} e^{(iur_n)},$$ (6)

where the scattering function $F(\vartheta)$ is

$$F(\vartheta) = \frac{i}{2k} \sum_{n}^{\infty} (2n+1)(1+R_n)P_n(\cos \vartheta)$$ (7)

and $P_n(\cos \vartheta)$ are Legendre polynomials, where $u = k_0 - k$, k, and k_0 are the wave vectors of the plane and scattered waves. The sum in Eq. (6) can be split into two terms:

$$\sum_{n=1}^{N} e^{(iur_n)} = \left[N + \sum_{n \neq m}^{N} e^{(iur_{mn})} \right].$$ (8)

The first term on the right-hand side of Eq. (8) is the number of dots in volume V and represents the scattering of phonons from quantum dots when they act as independent scattering centers. We refer to this as the *incoherent* scattering term. The second term on the right-hand side of the Eq. (8) represents the cooperative scattering action of the quantum dots. We refer this to the *coherent* scattering term, in analogy with the terminology adopted in acoustics.[24] An appearance of the coherent scattering in the cross plane direction is caused by the dot ordering in the layers.

In general, the problem of finding the total cross section, σ_V, can be done only numerically. Averaging of the scattering effects produced by a single quantum dot layer can result in a significant simplification of the calculation procedure. In some special cases, such as the *weak scattering density limit* described in Ref. 25, the averaging can be done over the Fresnel zones. The rescattering from all scatters in a given zone will be, on average, equal in magnitude but opposite in sign from the contribution of the presending zone. Following this stationary phase approach, only scatters within the first Fresnel zone contribute to the transmitted wave field. By definition these scatters radiate in phase with the background wave field, which means that the precise location of the scatter is of minor importance. The discrete distribution of the scatters can be replaced by a smooth scatter density, ν. We use the result obtained in Ref. 26 for the transmission coefficient of a single layer:

$$T = \left(1 - i \frac{\nu_s}{2k} f(0) \right),$$ (9)

where ν_s is the sheet dot density in the layer. The weak scattering density limit is defined by the requirement $|\nu f(0)/k^2| \ll 1$, which is well satisfied due to the finite acoustic mismatch between Si and Ge up to 10^{10}-dot/cm^2 density.

The effects of scattering on quantum dots affect other relaxations times via phonon dispersion modification. In the cross-plane direction the increased phonon scattering modifies the phonon dispersion in such a way that acoustic phonons travel with a group velocity different from the one in bulk. The problem of wave dispersion in a medium containing a number of scatters has been intensively studied for
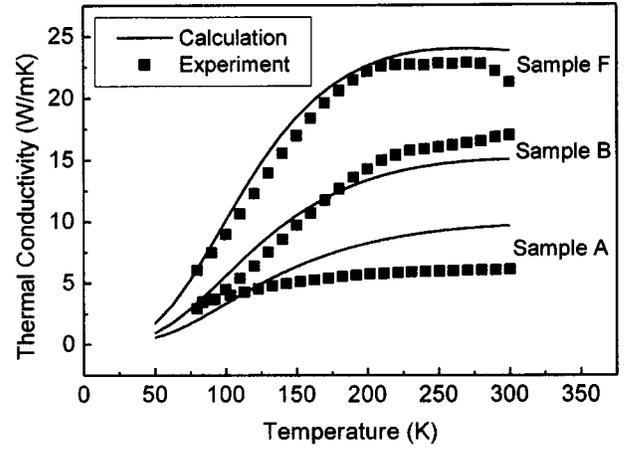
FIG. 5. Comparison of experimental and calculated thermal conductivity as a function of measurement temperature for three samples.

a long time.[25–27] The detailed discussion can be found in Ref. 28, where phonon dispersion modification due to the scattering on quantum dots had been taken into account in order to simulate in-plane phonon transport in a quantum dot superlattice.

The procedure calculating the cross-plane thermal conductivity consists of a number of steps. First, we calculate the single dot scattering function [Eqs. (5)–(7)]. Then, we calculate the total cross section for the quantum dot superlattice taking into account dot ordering in space [Eqs. (6)–(9)]. Next, we calculate the set of relaxation times using Eq. (2), taking into account dispersion modification. Finally, we obtain the lattice thermal conductivity using Eq. (1).

The total scattering on quantum dots in the considered temperature range exceeds those caused by phonons and isotopes. This results in a significant cross-plane lattice conductivity decrease as well as modification of the thermal conductivity temperature dependence. In Fig. 5, we show a plot of thermal conductivity versus temperature for SiGe quantum dot superlattice samples A, B, and F. It is clear that the calculated temperature dependence of thermal conductivity for all samples are in good agreement with the experimental data. The results of numerical simulation show the same shift of the superlattice K-T curve peak position in comparison with the curve from bulk materials in Fig. 2. The good agreement between the calculated and experimental data validates our approach based on the continuum model approximation and the assumption that the thermal phonon wave can be represented by a sum of plane waves affected by the scattering on acoustically mismatched obstacles.

We have demonstrated that a simple model taking into consideration the relaxation time approximation can explain the large reduction in the thermal conductivity of quantum dot samples compared with bulk. Moreover, it also explains the observed variation in thermal conductivity for different samples by considering the variation of dot base diameter, quantum dot density, and Si/Ge interdiffusion effect that smooths an acoustic mismatch between silicon and SiGe dots. The question now arises as to which of the three physical parameters plays a more important role in determining
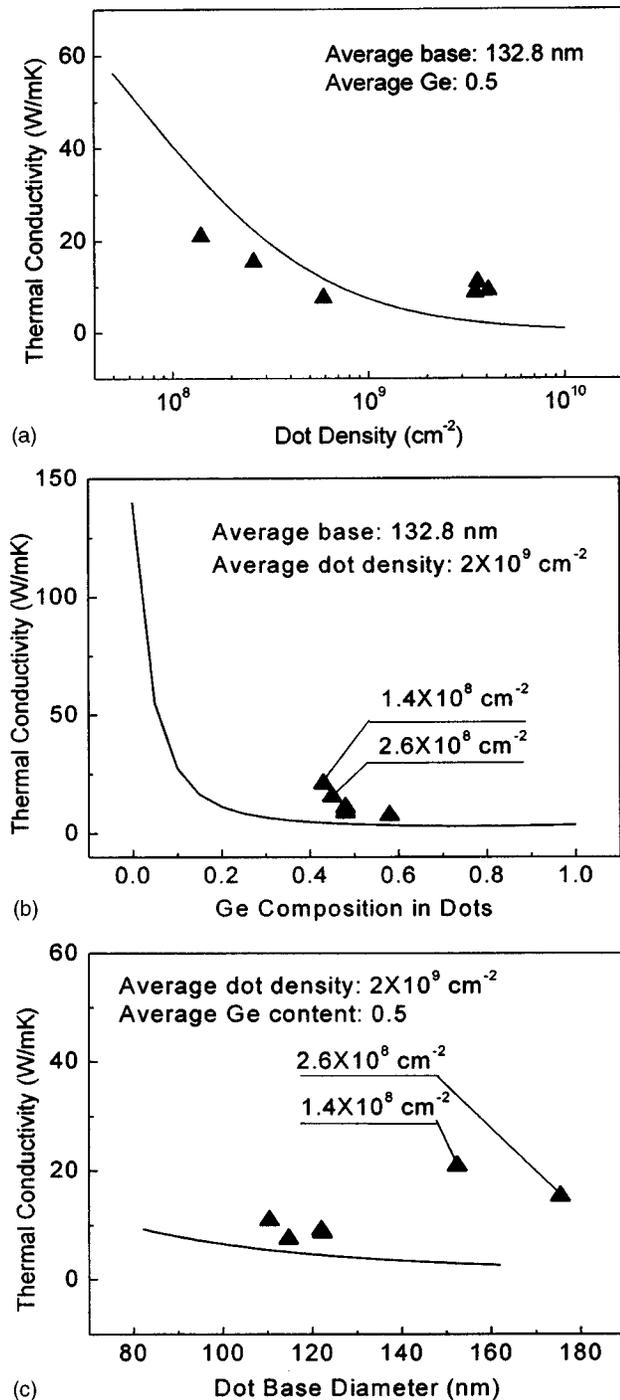
FIG. 6. Room-temperature thermal conductivity as a function of (a) dot density, (b) Ge composition in quantum dots, and (c) dot base diameter. For each curve we varied only one parameter (x axis). Dot height (14 nm) and interlayer distance (20 nm) are the same for all points in the graph.

the thermal conductivity. To clarify the relative importance, in Fig. 6 we have plotted lattice thermal conductivity as a function of the dot density, Ge composition in quantum dots, and dot base diameter, respectively. The solid curves are calculated data and the triangle symbols are experiment data. For each plot, on one parameter was varied. The dot height (14 nm) and interlayer distance (20 nm) are the same for all

points in the graph. As seen in Fig. 6, the calculation shows that an increase of dot density as well as Ge content in the quantum dots significantly decreases the lattice thermal conductivity, while an increase in dot base diameter has a weaker impact in reducing the thermal conductivity. The explanation for this comes from Eqs. (5)–(8), where an increase in dot density enhances both *coherent* and *incoherent* terms produced by the quantum dot ensemble [Eq. (8)], while an increase in Ge content enhances acoustic mismatch between the dot and host material ($\rho c / \rho_e c_e$), and thus, increases the scattering produced by a single dot [Eq. (5)]. An increase in growth temperature results in Ge diffusion out of dots, decreasing the dot-host material acoustic mismatch. Samples grown at lower temperature contain more Ge inside the dot, and thus, exhibit lower thermal conductivity. An increase in the dot base diameter also results in the enhancement of single dot scattering, therefore decreasing the thermal conductivity. Nevertheless, a relatively small dot size variation (see Table I) makes the effect of this parameter minor in comparison with the other two. This can also be concluded from the comparison with the experimental data points. In Fig. 6(c), the experimental data points do not follow the trend of the calculated data because other parameters, such as dot density, play a more dominant role in determining the thermal conductivity. To emphasize this, in Fig. 6(c) we have highlighted the dot density for two specific samples which have dot density that are one order of magnitude lower than the average dot density used for the calculation. Because all of our quantum dot samples have a Ge composition close to 0.5 in the dots, we do not observe the experimental data following the calculated curve in a large region, especially in the dramatic thermal conductivity change region for Ge composition between 0 to 0.2. Nevertheless, most of the experiment data fit the calculated curve except that two points deviate from the curve because of their small dot densities. In Fig. 6(a), we observe fairly good agreement between the experimental data and the calculation, where we change the dot density only and fix all other physical parameters.

IV. CONCLUSION

In summary, we report the temperature-dependent thermal conductivity of different Ge quantum dot superlattices and present a theoretical explanation for the obtained results. It is found that the thermal conductivity of the Ge quantum dot superlattices is significantly reduced compared with the bulk values of Si and Ge. A simple model based on the relaxation time approximation explains not only this large reduction but also the variation in thermal conductivity among the different quantum dot samples.

*Email address: jianlin@ee.ucr.edu

[1] O. P. Pchelyakov, Yu. B. Bolkhovityanov, A. V. Dvurechenskii, A. I. Nikiforov, A. I. Yakimov, and B. Voigtlander, Thin Solid Films **367**, 75 (2000).

[2] K. Eberl, O. G. Schmidt, R. Duschl, O. Kienzle, E. Ernst, and Y. Rau, Thin Solid Films **369**, 33 (2000).

[3] J. L. Liu, W. G. Wu, A. Balandin, G. L. Jin, and K. L. Wang, Appl. Phys. Lett. **74**, 185 (1999).

[4] P. Boucaud, V. Le Thanh, S. Sauvage, D. De'barre, and D. Bouchier, Appl. Phys. Lett. **74**, 401 (1999).

[5] A. I. Yakimov, A. V. Dvurechenskii, A. I. Nikiforov, and Yu. Yu. Proskuryakov, J. Appl. Phys. **89**, 5676 (2001).

[6] L. D. Hicks and M. S. Dresselhaus, Phys. Rev. B **47**, 12 727 (1993).

[7] T. Koga, S. B. Cronin, M. S. Dresselhaus, J. L. Liu, and K. L. Wang, Appl. Phys. Lett. **77**, 1490 (2000).

[8] G. D. Mahan, Semicond. Semimetals **71**, 157 (2001).

[9] M. S. Dresselhaus, Y. M. Lin, S. B. Cronin, O. Rabin, M. R. Black, G. Dresselhaus, and T. Koga, Semicond. Semimetals **71**, 1 (2001).

[10] T. C. Harman, P. J. Taylor, L. D. Spears, and M. P. Walsh, J. Electron. Mater. **29**, L1 (2000).

[11] G. Chen, Semicond. Semimetals **71**, 203 (2001).

[12] R. Venkatasubramanian, Semicond. Semimetals **71**, 175 (2001).

[13] X. Fan, G. Zeng, C. LaBounty, J. E. Bowers, E. Croke, C. C. Ahn, S. Huxtable, A. Majumdar, and A. Shakouri, Appl. Phys. Lett. **78**, 1580 (2001).

[14] A. Milekhin, N. P. Stepina, A. I. Yakimov, A. I. Nikiforov, S. Schulze, and D. R. T. Zahn, Appl. Surf. Sci. **175**, 629 (2001).

[15] J. L. Liu, G. Jin, Y. S. Tang, Y. H. Luo, K. L. Wang, and D. P. Yu, Appl. Phys. Lett. **76**, 586 (2000).

[16] W. L. Liu, T. Borca-Tasciuc, G. Chen, J. L. Liu, and K. L. Wang, J. Nanosci. Nanotechnol. **1**, 37 (2001).

[17] J. L. Liu, A. Khitun, K. L. Wang, T. Borca-Tasciuc, W. L. Liu, G. Chen, and D. P. Yu, J. Cryst. Growth **227**, 1111 (2001).

[18] J. L. Liu, J. Wan, Z. M. Jiang, A. Khitun, K. L. Wang, and D. P. Yu, J. Appl. Phys. **92**, 6804 (2002).

[19] T. Borca-Tasciuc, A. R. Kumar, and G. Chen, Rev. Sci. Instrum. **72**, 2139 (2001).

[20] S. M. Lee and D. G. Cahill, J. Appl. Phys. **81**, 2590 (1997).

[21] G. P. Srivastava, *The Physics of Phonons* (Adam Hilger, New York, 1990), p. 128.

[22] P. G. Klemens, in *Solid State Physics*, edited by F. Seitz and Turnbull (Academic, New York, 1958), Vol. 7, p. 1.

[23] A. Khitun, A. Balandin, J. L. Liu, and K. L. Wang, J. Appl. Phys. **88**, 696 (2000).

[24] P. M. Morse and H. Feshbach, *Methods of Theoretical Physics* (McGraw-Hill, New York, 1953), Part II, pp. 418–430.

[25] P. C. Waterman and R. Truell, J. Math. Phys. **2**, 512 (1961).

[26] J. Groenenboom and R. Snieder, J. Acoust. Soc. Am. **98**, 3482 (1995).

[27] M. Lax, Rev. Mod. Phys. **23**, 287 (1951).

[28] A. Khitun, A. Balandin, J. L. Liu, and K. L. Wang, Superlattices Microstruct. **30**, 1 (2001).